

Electronic structures of Ba-on-Alq₃ interfaces and device characteristics of organic light-emitting diodes based on these interfaces

Jong Tae Lim,¹ Geun Young Yeom,^{1,a)} Kyuwook Lhm,² and Tai-Hee Kang²

¹*School of Advanced Materials Science and Engineering, Sungkyunkwan University, Suwon 440-746, Republic of Korea*

²*Department of Physics and Pohang Accelerator Laboratory, POSTECH, Pohang 790-784, Republic of Korea*

(Received 28 January 2009; accepted 4 February 2009; published online 20 April 2009)

The device performance of organic light-emitting diodes was significantly improved by inserting a Ba coverage (Θ_{Ba}) of 1 nm between tris(8-quinolinolato)aluminum (III) (Alq₃) and the cathode. This improvement was attributed to the lowering of the electron-injecting barrier height that was induced by the formation of a new gap state from an interfacial chemical reaction, as well as band bending due to Fermi level pinning. However, the device with Θ_{Ba} above 1 nm showed poor device performance. The spectroscopic results indicated that the Alq₃ molecules started to decompose by the reaction between Ba and the phenoxide moiety of the molecule. © 2009 American Institute of Physics. [DOI: 10.1063/1.3106604]

I. INTRODUCTION

One of the fundamental issues in optimizing the performance of organic light-emitting diodes (OLEDs) is to improve electron injection through a cathode/organic interface.¹⁻³ The electron affinities of electron-transporting materials (ETMs) such as tris(8-quinolinolato)aluminum (III) (Alq₃) are much lower than the work function (WF) of typical cathode materials such as Al, Ag, and Au.² It forms a rather high barrier height for an electron injection ($\Phi_{\text{B}}^{\text{N}}$) (Ref. 2) at the cathode/ETM interfaces, leading to high-operation voltages and poor long-term stability. The light-emission efficiency of OLEDs is limited by the number of injected electrons because most organic semiconductors are *p*-type and electron mobilities are in general lower than hole mobilities. Therefore, the efficient electron-injecting interface is the key to improving the operation voltage and emission efficiency.⁴ Lower $\Phi_{\text{B}}^{\text{N}}$ has been obtained for lower WF metals such as Cs,⁵ Mg,⁶ and Ca.⁷ In these cathode/ETM interfaces, the following two aspects are the important issues: first, the energy level alignment at the interface, and second, the interfacial chemical reaction. The former is important in the aspect of electron injection, while the latter is essential for understanding the chemical process that leads to the degradation of the device. The interfacial electronic structure of the devices plays an important role in determining their luminous efficiency and lifetime.

To improve device performance, top-emitting OLEDs (TEOLEDs) with a Ba/Au cathode were fabricated with different thicknesses of Ba coverage (Θ_{Ba}) on Alq₃ and their electrical and optical properties were investigated. In addition, the mechanism of the variation in device properties as a function of Θ_{Ba} on Alq₃ for the TEOLEDs was studied.

II. EXPERIMENTAL PROCEDURES

The electronic structure of the Ba-on-Alq₃ interfaces was examined by using x-ray photoemission spectroscopy (XPS), ultraviolet photoemission spectroscopy (UPS), and near-edge x-ray absorption fine structure (NEXAFS) spectroscopy at the 4B1 beam line in the Pohang Accelerator Laboratory (Korea). All measurements and depositions were performed in an ultra-high vacuum system, consisting of a main analysis chamber (approximately 5×10^{-10} Torr) and a sample preparation chamber (approximately 5×10^{-9} Torr). All samples were prepared *in situ* by sequential thermal evaporation on a Si wafer and all thicknesses were determined by timed depositions calibrated using a quartz-crystal microbalance. In the XPS studies, incident photon energies of 880, 650, and 550 eV were used to obtain the core level spectra of O 1s, N 1s, and Ba 3d, respectively. For the UPS measurements, the He I (21.2 eV) line from a UV source was used. The photoemission onset reflecting the vacuum level at the surface of all samples was measured by biasing the samples at -20 V. The incident photon energy was calibrated by measuring the Au 4f level of a clean Au surface. In the NEXAFS analyses, nitrogen *K*-edge (387–417 eV) spectra were measured at a photon incident angle of 45°.

The TEOLED was composed of glass/Ag (150 nm)/tin-doped indium oxide (ITO) (125 nm)/4,4',4''-tris(2-naphthylphenyl-1-phenylamino)triphenylamine (2-TNATA, 30 nm)/4,4'-bis[N-(1-naphthyl)-N-phenyl-amino]-biphenyl (NPB, 18 nm)/Alq₃ (62 nm)/Ba/Au (20 nm), with Θ_{Ba} values of 0 nm (device 0), 1 nm (device 1), 2 nm (device 2), and 3 nm (device 3). All devices were fabricated by evaporation on glass/Ag/ITO substrates and the current density-voltage-luminance characteristics were also measured using a Keithley 2400 electrometer, a photodiode (Oriol 71608), and a Keithley 485 picoammeter.

III. RESULTS AND DISCUSSION

Figure 1 shows the current density-voltage characteristics for devices 0–3. The turn-on voltages (voltage at

^aElectronic mail: gyeom@skku.edu. FAX: +82-31-299-6565.

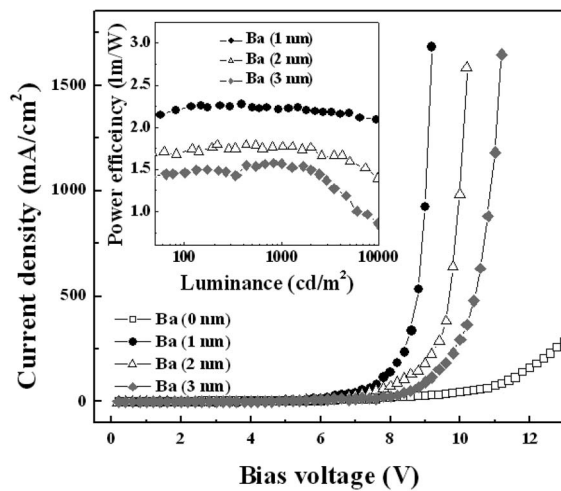


FIG. 1. Current density curves as a function of bias voltage. The inset shows the power efficiency-luminance curves. The devices were composed of glass/Ag (150 nm)/ITO (125 nm)/2-TNATA (30 nm)/NPB (18 nm)/Alq₃ (62 nm)/Ba (*x* nm)/Au (20 nm). (Ba thickness of devices 0–3=0, 1, 2, and 3 nm, respectively).

0.1 cd/m², V_T) of devices 1–3 were all 2.8 V but device 0 without Ba showed a higher V_T value of 5.4 V. Meanwhile, at the current density of approximately 100 mA/cm², the bias voltages of devices 0–3 were 11.4, 7.6, 8.2, and 9.0 V, respectively, as seen in Fig. 1. When the 1-nm-thick Ba was inserted between the cathode and Alq₃, as shown in device 1, the power consumption (η_{PC}) of the devices was decreased by 33% compared to the device without Ba. However, η_{PC} of devices 2 and 3 was again increased. The inset of Fig. 1 shows the power efficiency (η_{PE}) characteristics as a function of luminance for devices 1–3. At the luminance of 100 cd/m² (L_{100}), device 1 showed the highest η_{PE} of 2.3 lm/W. However, as Θ_{Ba} was increased to 2 and 3 nm, η_{PE} was reduced to 1.7 and 1.5 lm/W, respectively. These η_{PC} and η_{PE} results indicated that the device performance largely depends on Θ_{Ba} . The device performance was maximized with a 1-nm-thick Θ_{Ba} , but deteriorated as Θ_{Ba} was increased above 1 nm. To gain further insight on the mechanism involved in the enhancement of the device performance, the electronic structures of the Ba-on-Alq₃ interfaces were investigated as a function of Θ_{Ba} .

Figure 2(a) shows the spectral region around the highest occupied molecular orbitals (HOMOs) of the Ba-on-Alq₃ interfaces in the UPS spectra, as a function of Θ_{Ba} ranging from 0 to 20 nm on Alq₃. Also, Fig. 2(b) in the UPS spectra shows the photoemission onset measured at the Ba-on-Alq₃ interfaces as a function of Θ_{Ba} ranging from 0 to 20 nm on Alq₃ with a sample bias of -20 V, reflecting the WF shifts of Alq₃ achieved by Ba adsorption. In Fig. 2(a), all Alq₃ molecular orbital features were shifted to a higher binding energy with increasing Θ_{Ba} . The energy shift of the HOMO peak was maximized at Θ_{Ba} of 0.05 nm and the binding energy remained approximately 0.4 eV higher than that of the pristine Alq₃, as shown in Fig. 2(a). This lowering of the HOMO levels indicates that Φ_B^N is lowered as 0.4 eV when compared to that of the pristine Alq₃, as seen in the proposed energy diagram of the Ba-on-Alq₃ interfaces at Θ_{Ba} between

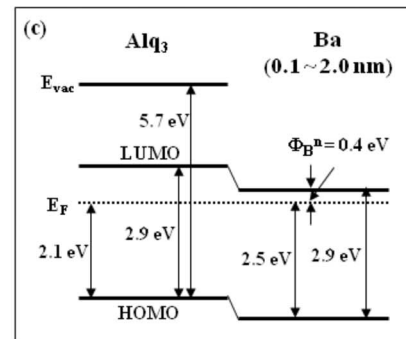
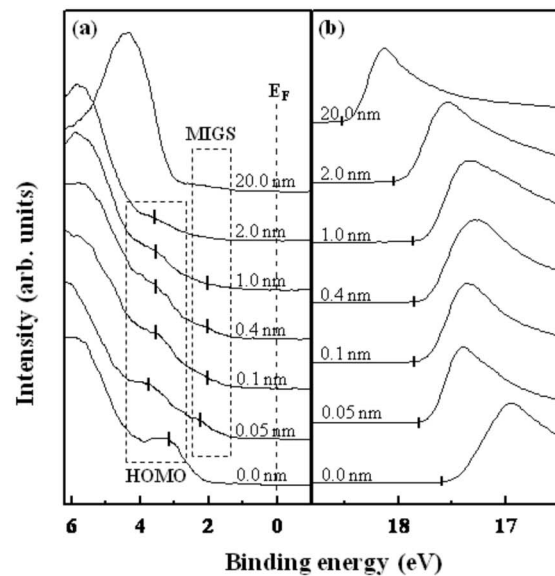


FIG. 2. UPS of the Ba-on-Alq₃ interfaces show (a) spectral region around the Alq₃ HOMO and the (b) onset of photoemission with a sample bias of -20 V, indicating the WF as a function of Θ_{Ba} on Alq₃, respectively. The values in the figures indicate Θ_{Ba} . (c) shows the proposed energy band diagrams of the Ba-on-Alq₃ interfaces at Θ_{Ba} between 0.1 and 2.0 nm.

0.1 and 2.0 nm in Fig. 2(c).² Here, the ionization potential and the energy band gap (E_g) of the pristine Alq₃ in Fig. 2(c) were taken as 5.7 and 2.9 eV, respectively.² In addition, as shown in Fig. 2(a), the metal-induced gap state (MIGS),⁸ which is roughly a free-electron-like, metal wave function penetrating into the organic semiconductor side, was observed at the forbidden energy gap of approximately 1.5 eV above the HOMO of Alq₃. The band between Alq₃ and the cathode was realigned due to the introduced MIGS and WF difference.⁹ In fact, a new gap state has also been observed in several interfaces between a low WF metal (e.g., Li, Na, K, Ca, and Mg) and Alq₃.¹⁰

Figure 3 shows the WF shift ($\Delta\Phi = \Phi_{Alq_3} - \Phi_{Ba-on-Alq_3}$) from Fig. 2(a) and the HOMO level shift ($e_0\Delta V_s = \text{HOMO}_{Alq_3} - \text{HOMO}_{Ba-on-Alq_3}$) from Fig. 2(b) as a function of Θ_{Ba} ranging from 0 to 2 nm. The HOMO level shifts can be expressed by $e_0\Delta V_s = \Delta I - \Delta\Phi$,² where ΔI is the ionization energy change. The band bending ($e_0\Delta V_s$) marked by the filled squares was not equal to $\Delta\Phi$ ($e_0\Delta V_s \neq \Delta\Phi$) and the definite differences between $e_0\Delta V_s$ and $\Delta\Phi$ indicate that the HOMO-level shifts did not simply originate from the WF difference but may have resulted from a possible chemical reaction between Alq₃ and cathode. These results suggest

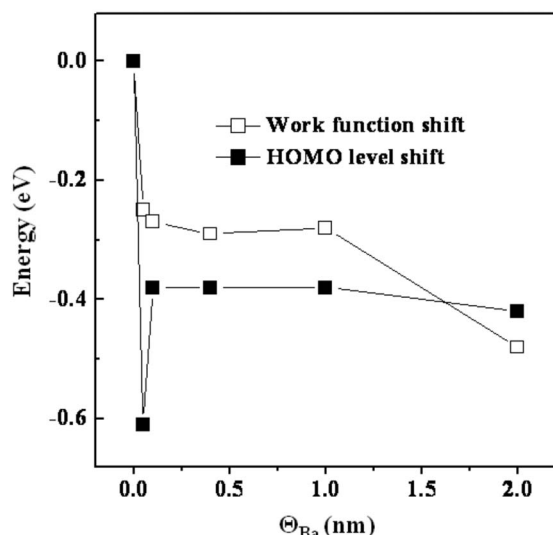


FIG. 3. WF shift (open squares) of $\Phi_{\text{Alq}_3} - \Phi_{\text{Ba-on-Alq}_3}$ and the HOMO level shift (closed squares) of $\text{HOMO}_{\text{Alq}_3} - \text{HOMO}_{\text{Ba-on-Alq}_3}$ as a function of Θ_{Ba} on Alq_3 in the pristine Alq_3 and Ba-on-Alq_3 interfaces.

that the lowering of the HOMO level in the Ba-on-Alq_3 interfaces was due not only to the band bending by Fermi level pinning, but also to the chemical modification of the Alq_3 molecules by the excess electrons of the Ba metal. Moreover, the presence of MIGS in the Ba-on-Alq_3 interfaces, as shown in Fig. 2(a), is further evidence for the chemical reaction between Ba and Alq_3 .

Figure 4(a) shows the evolution of the O 1s electron density curves (EDCs) as a function of Θ_{Ba} ranging from 0 to 10 nm on Alq_3 (100 Å), as measured by XPS. For $\Theta_{\text{Ba}} = 0$ Å, the O 1s core-level EDC was symmetrical in shape and was composed of a single component, indicating a clean Alq_3 film. The single component of the O 1s EDC was initially shifted to a lower binding energy of 530.3 eV [Alq_3 radical anion formed by electron charge transfer (ECT) from Ba] until $\Theta_{\text{Ba}} = 1.0$ nm, compared with the pristine Alq_3 of 531.6 eV. From $\Theta_{\text{Ba}} = 2.0$ nm, a O 1s peak of 527.3 eV (decomposition by Al–O bond breaking) with low intensity began to appear at a lower binding energy, and the intensity of

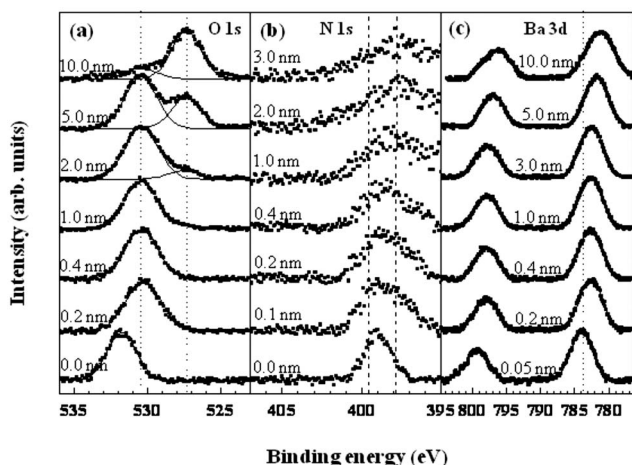


FIG. 4. The evolution of XPS (a) O 1s, (b) N 1s, and (c) Ba 3d core level EDCs as a function of Θ_{Ba} on Alq_3 . The values in the figures indicate Θ_{Ba} .

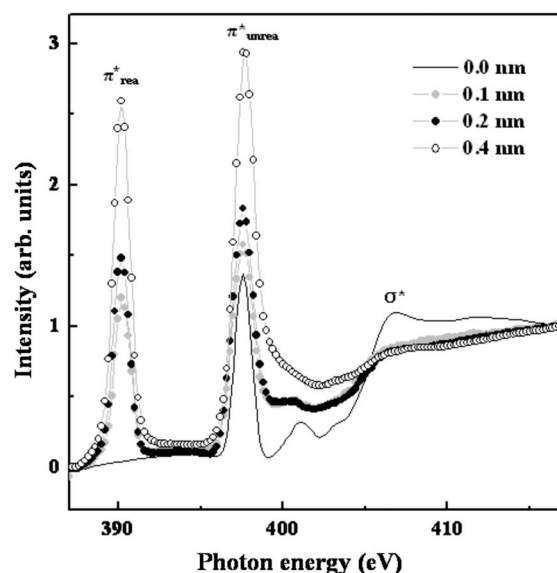


FIG. 5. NEXAFS spectra at the N K-edge of the Ba-on-Alq_3 interfaces over a Θ_{Ba} range from 0 to 0.4 nm.

the 527.3 eV peak was further increased at $\Theta_{\text{Ba}} = 5.0$ nm. The peak shift to a lower binding energy was caused by a decrease in the Coulomb potential between the nuclei and the electrons of the valence band as a result of the increased electron density at the valence band of O atoms due to an electron provided by Ba.²

Meanwhile, Choong *et al.*¹¹ reported that the binding energy difference between an Alq_3 radical component and a decomposition component in the Ca/Alq_3 interface was 2.0 eV in the XPS spectra of O 1s. The large peak shift of 3.0 eV between the Alq_3 radical component and the decomposition component, as shown in Fig. 4(a), indicates bond breaking between the Al and O atoms in the Alq_3 molecule. Therefore, the peak at a low binding energy of 527.3 eV was attributed to the appearance of a metallic Alq_3 component that was decomposed by the large ECT from Ba for higher Θ_{Ba} . Figure 4(b) shows the N 1s core level EDCs as a function of Θ_{Ba} ranging from 0 to 3 nm. Even as early as $\Theta_{\text{Ba}} = 0.1$, a decomposition component (around 398.0 eV) reacting with Ba was observed with the Alq_3 radical component (around 399.6 eV). This shows that Ba interacts with N before O, which is reasonable given that the Al–N bond is the weakest in the molecule. Considering the dependence of the device characteristics shown in Fig. 1 on Θ_{Ba} , the formation of the decomposition component in the N XPS spectra did not affect the device performance at all Θ_{Ba} . However, the emergence of the decomposition component in the O XPS spectra provides a direct cause of the poor device performance at Θ_{Ba} above 1 nm. Figure 4(c) shows the 3d peaks of Ba EDC. The Ba $3d_{5/2}$ peak was shifted to the highest binding energy of 783.8 eV at the lowest Θ_{Ba} of 0.05 nm and then shifted slowly to a low binding energy of 781.1 eV with increasing Θ_{Ba} . This result means that the largest ECT from Ba to Alq_3 occurred at the lowest Θ_{Ba} of 0.05 nm and that the unreacted, excess Ba atoms were stacked on the interface with increasing Θ_{Ba} .

Figure 5 shows the NEXAFS spectra at the N K-edge of

the Ba-on-Alq₃ interfaces as Θ_{Ba} ranges from 0 to 0.4 nm. NEXAFS spectroscopy shows the resonance features induced by a transition from the initial state (core level) to the final state (vacant level) and can be used to obtain information on the unoccupied state. Curioni *et al.*¹² reported peaks at 397.6, 401.2, and 406.8 eV in the pristine Alq₃ due to the transitions of electrons from the N 1s level to the lowest unoccupied molecular orbital (LUMO), LUMO+2 (and LUMO+3), and many σ^* , respectively. The spectrum from pristine Alq₃ was in good agreement with the results of Curioni *et al.*¹² Interestingly, new resonance peaks appear at 390.2 eV upon Ba adsorption.

The peaks at 390.2 and 397.6 eV, which were induced by the transition to the LUMO levels consisting of π^* unoccupied states, were attributed to π_{rec}^* (species of N atom reacted with Ba) and π_{unrec}^* (species of N atom unreacted with Ba), respectively. The difference (7.4 eV) in the large photon energy between π_{rec}^* and π_{unrec}^* was interpreted as being caused by the change in the final state, because the N 1s core level does not show any strong feature related with the chemical modification, as shown in Fig. 4(b). The appearance of a π_{rec}^* peak even at Θ_{Ba} of 0.1 nm on Alq₃ indicated that the orbitals involved with ECT were mainly localized at the pyridyl ring¹³ rather than the phenoxide ring¹³ on the 8-quinolinolato ligand composing the Alq₃ molecule.

IV. CONCLUSIONS

In summary, we investigated the mechanism of the improved device performance achieved by incorporating Ba in the cathode structure. At Θ_{Ba} of 1 nm, the device performance was enhanced by reducing the HOMO level by about 0.4 eV, as shown in the UPS spectra. This reduction was due to the MIGS formed by chemical reaction as well as the band bending formed by Fermi level pinning between Ba and Alq₃. Although the $\Phi_{\text{B}}^{\text{N}}$ values at Θ_{Ba} of 1.0 and 2.0 nm were almost identical, the interface chemistry largely depended on Θ_{Ba} , as shown in the MIGS, reactive species in the XPS

spectra (O 1s and N 1s), and the NEXAFS spectra at the N K-edge. The formation of a stable radical anion at $\Theta_{\text{Ba}} = 1.0$ nm enhanced the device performance of the TEOLED but the appearance of a metallic component from $\Theta_{\text{Ba}} = 2.0$ nm degraded the device performance due to Al–O, rather than Al–N, bond breaking in Ba-on-Alq₃ interfaces.

ACKNOWLEDGMENTS

This research was supported by a grant (PAD-4) from the Information Display R&D Center, one of the 21st Century Frontier R&D Program funded by the Ministry of Knowledge Economy of Korean government. Also, this work was supported by the Pohang Accelerator Laboratory in Korea.

¹L.-L. Chua, J. Zaumseil, J.-F. Chang, E. C.-W. Ou, P. K.-H. Ho, H. Stiringhaus, and R. H. Friend, *Nature (London)* **434**, 194 (2005).

²H. Ishii, K. Sugiyama, E. Ito, and K. Seki, *Adv. Mater. (Weinheim, Ger.)* **11**, 605 (1999).

³K.-Y. Wu, Y.-T. Tao, and H.-W. Huang, *Appl. Phys. Lett.* **90**, 241104 (2007).

⁴L. C. Palilis, M. Uchida, and Z. H. Kafafi, *IEEE J. Sel. Top. Quantum Electron.* **10**, 79 (2004).

⁵J.-H. Lee, M.-H. Wu, C.-C. Chao, H.-L. Chen, and M.-K. Leung, *Chem. Phys. Lett.* **416**, 234 (2005).

⁶R. Q. Zhang, W. C. Lu, C. S. Lee, L. S. Hung, and S. T. Lee, *J. Appl. Phys.* **116**, 8827 (2002).

⁷A. Curioni, W. Andreoni, R. Treusch, F. J. Himpsel, E. Haskal, P. Seidler, C. Heske, S. Kakar, T. van Buuren, and L. J. Terminello, *Appl. Phys. Lett.* **72**, 1575 (1998).

⁸M. Kiguchi, R. Arita, G. Yoshikawa, Y. Tanida, S. Ikeda, S. Entani, I. Nakai, H. Kondoh, K. Saiki, and H. Aoki, *Phys. Rev. B* **72**, 075446 (2005).

⁹J. Tersoff, *Phys. Rev. Lett.* **52**, 465 (1984).

¹⁰C. Shen, I. G. Hill, A. Kahn, and I. Schwartz, *J. Am. Chem. Soc.* **122**, 5391 (2000).

¹¹V.-E. Choong, M. E. Mason, C. W. Tang, and Y. Gao, *Appl. Phys. Lett.* **72**, 2689 (1998).

¹²A. Curioni, W. Andreoni, R. Treusch, F. J. Himpsel, E. Haskal, P. Seidler, C. Heske, S. Kakar, T. van Buuren, and L. J. Terminello, *Appl. Phys. Lett.* **72**, 1575 (1998).

¹³C. H. Chen and J. Shi, *Coord. Chem. Rev.* **171**, 161 (1998).